Quasisymmetry-Constrained Spin Ferromagnetism in Altermagnets

Mercè Roig,[1,2] Yue Yu,[2] Rune C. Ekman,[1] Andreas Kreisel,[1] Brian M. Andersen,[1] and Daniel F. Agterberg[2]
[1]Niels Bohr Institute, University of Copenhagen, DK-2100 Copenhagen, Denmark
[2]Department of Physics, University of Wisconsin–Milwaukee, Milwaukee, Wisconsin 53201, USA

(Received 16 December 2024; revised 29 April 2025; accepted 2 June 2025; published 1 July 2025)

Altermagnets break time-reversal symmetry, and their spin-orbit coupling (SOC) allows for an anomalous Hall effect (AHE) that depends on the direction of the Néel ordering vector. The AHE and the ferromagnetic spin moment share the same symmetry and hence are usually proportional. However, density functional theory (DFT) calculations find that the AHE exists with negligible ferromagnetic spin moment for some compounds, whereas it reaches sizable values for other altermagnets. By examining realistic minimal models for altermagnetism in which the DFT phenomenology is captured, we uncover a general SOC-enabled quasisymmetry, the uniaxial spin space group, that provides a natural explanation for the amplitude of the ferromagnetic spin moment across the vast range of different altermagnetic materials. Additionally, we derive analytic expressions for the magnetic anisotropy energy, providing a simple means of identifying the preferred Néel vector orientation for altermagnets.

DOI: 10.1103/839n-rckn

Introduction—The Hall effect has been a frontier theme in condensed matter physics for more than half a century. Fundamental understanding of the quantized Hall conductance and the anomalous Hall effect (AHE) has helped pave the way for topological classifications of quantum matter and the importance of Berry curvature in transport properties [1–7]. The discovery of altermagnetism (AM) and its associated large antiferromagnetic AHE is yet another testimony to this development [8–17], which may open new opportunities for devices utilizing dissipationless transport and spintronics technologies [5,18–22].

The AHE in AM, which we describe here as an intraunit cell Néel order, is only nonzero for certain directions of the Néel vector and in the presence of relativistic spin-orbit coupling (SOC). This, in addition, induces weak ferromagnetism (FM), which satisfies the same symmetry properties as the AHE [23,24]. This implies that, in principle, FM and AHE share the same dependence on the orientation of the Néel vector [21,25,26]. However, from density functional theory (DFT) it is found that the relative amplitude of the AHE transport coefficient and the FM spin moment depend strongly on the particular AM material under investigation. For example, for RuO_2 and MnTe, DFT finds a large AHE of 40 S/cm and 300 S/cm, respectively, while RuO_2 has a nearly zero FM moment (that we estimate is of the order 10^{-7} μ_B) and Mn in MnTe has 10^{-4} μ_B [17,18,27]. In the case of MnTe and RuO_2, weak FM was also reported experimentally [16,28], though the AM ground state of the latter material is still debated [29,30]. A weak FM spin moment has also been identified by DFT in CrSb [31]. By contrast, in other AM, such as $FeSb_2$, DFT finds a large AHE of 143 S/cm [32,33], and our calculations estimate a moderate FM moment of 0.03 μ_B. Similarly, the material RuF_4 has also been predicted by DFT to exhibit a large FM spin moment of 0.22 μ_B on the Ru sites [34]. These results suggest that, while the AHE is generically large when allowed by symmetry, the corresponding FM moment is strongly dependent on the AM state, and this is poorly understood.

To gain deeper insight into the interplay between the AHE, the FM moment, and the AM state, it is crucial to analyze the role of SOC using realistic models. Here, by examining realistic microscopic models for AM in which the DFT phenomenology is captured [35], we identify which AM states have a large SOC induced AHE but a small FM spin moment and find good agreement with DFT results. In addition, we find that our model-based results are more generally valid. Specifically, they apply to all microscopic theories in which AM appears as a consequence of the exchange interaction. To show this, we identify a general SOC-enabled quasisymmetry [36,37], a uniaxial spin space group, that establishes for which AM symmetries the symmetry-allowed FM is large or vanishingly small. Finally, the presence of SOC in AM breaks the spin-space degeneracy and leads to a preferred direction for the Néel vector. For example, DFT calculations have revealed that the moments are orthogonal to the *a*-*b* plane in RuO_2 [15], while in MnTe, $FeSb_2$, Nb_2FeB_2, and Ta_2FeB_2 the moments are predicted to be in-plane [27,32,38]. By examining analytic expressions for the Landau coefficients derived from realistic microscopic models, we elucidate how the structure of SOC allows the AM anisotropy energy to be understood.

Interplay between magnetization and AM Néel order—Introducing $\vec{N}$ as the intraunit cell Néel order and $\vec{M}$ as the magnetization, the general form of the free energy density

in the presence of SOC can be written as

$$F = \frac{a_N}{2}\vec{N}^2 + \frac{b_N}{4}\vec{N}^4 + \frac{a_M}{2}\vec{M}^2 - \vec{h}\cdot\vec{M} + c_{ij}M_iN_j + s_1(N_x^2 - N_y^2) + s_2(N_x^2 + N_y^2 - 2N_z^2), \quad (1)$$

where a_N, b_N, a_M, and c_{ij} are temperature-dependent Landau coefficients, $\vec{h}$ is an applied field, and s_1 and s_2 are the coefficients determining the magnetic anisotropy energy due to SOC. Note that the bilinear coupling between the two orders M_i and N_j is only allowed in the presence of SOC [23]. Without SOC, the spin space group rotations, $[R_S\|R_G]$, with spin space (R_S) and real space group operations (R_G) are uncoupled, which forces the bilinear coupling to vanish since $\vec{N}$ is nontrivial under pure R_G operations. In the magnetic space group, the rotations act simultaneously on both spaces, and therefore R_S and the rotation portion of R_G must be the same, allowing this bilinear coupling to be nonzero. Equation (1) describes orthorhombic or higher-symmetry point groups; for monoclinic groups see Supplemental Material (SM) [39].

The lowest order invariant coupling M_i and N_j can be determined from symmetry analysis. The magnetization $\vec{M}$ belongs to the axial vector irreducible representation (IR) Γ_A; see SM [39]. In contrast, $\vec{N}$ belongs to the IR $\Gamma_A \otimes \Gamma_N$, with Γ_N of the IR denoting the symmetry of the AM spin splitting. Hence, a coupling of M_i and N_j exists if the direct product $\Gamma_A \otimes \Gamma_A \otimes \Gamma_N$ contains the IR transforming trivially under all point group operations or, equivalently, there is a free energy invariant if $\Gamma_A \otimes \Gamma_A$ contains Γ_N [23]. In Table I we provide the form of the free energy invariants considering the relevant point groups and symmetries for the spin splitting identified in Ref. [35]. Note that, for C_{6h}, O_h and certain IRs Γ_N of D_{6h}, a bilinear coupling is not allowed, and therefore the coupling is of higher order. Following a similar procedure, the lowest order coupling between the magnetization and the Néel vector can also be identified [39,40] and is included in Table I.

Microscopic models—To investigate the dependence of the induced FM spin moment on the SOC strength, we initially consider the general form of the minimal model for AM from Ref. [35] and carry out a model-independent quasisymmetry-based analysis later. Thus, we start from the normal state Hamiltonian

$$H_0 = \varepsilon_{0,\mathbf{k}} + t_{x,\mathbf{k}}\tau_x + t_{z,\mathbf{k}}\tau_z + \tau_y\vec{\lambda}_{\mathbf{k}}\cdot\vec{\sigma}, \quad (2)$$

where τ_i represent sublattice and σ_i is the spin degrees of freedom. The specific form of the parameters entering the model depends on the space group, the point group, and the Wyckoff site symmetry. Here, $t_{x,\mathbf{k}}$ is an intersublattice hopping term, $\varepsilon_{0,\mathbf{k}}$ is the sublattice independent dispersion, and $\vec{\lambda}_{\mathbf{k}}$ is the SOC. The crystal asymmetric hopping term $t_{z,\mathbf{k}}$ exhibits a $\mathbf{k}$ dependence that transforms as the nontrivial IR Γ_N since it describes the local symmetry breaking from multipole moments [35,41,42].

TABLE I. Lowest order free energy invariant between M_i and N_j in the presence of SOC for different point groups P and IRs of the spin splitting Γ_N, with the function $f_{\Gamma_N}(\mathbf{k})$ transforming as Γ_N. The last column indicates if the M_i generated from the AM order parameter is linear order in the SOC, denoted by a check mark, or higher order in SOC, denoted by a cross.

P	Γ_N	$f_{\Gamma_N}(\mathbf{k})$	Lowest order invariant	M_i linear in SOC
C_{2h}	B_g	$\alpha k_x k_z + \beta k_y k_z$	$\alpha_1 N_x M_z$, $\alpha_2 N_y M_z$ $\alpha_3 N_z M_y$, $\alpha_4 N_z M_x$	✓
D_{2h}	B_{1g}	$k_x k_y$	$\alpha_1 M_x N_y + \alpha_2 M_y N_x$	✓
D_{2h}	B_{2g}	$k_x k_z$	$\alpha_1 M_y N_z + \alpha_2 M_z N_y$	✓
D_{2h}	B_{3g}	$k_y k_z$	$\alpha_1 M_z N_x + \alpha_2 M_x N_z$	✓
C_{4h}	B_g	$\alpha(k_x^2 - k_y^2)$ $+\beta k_x k_y$	$M_x N_y + M_y N_x$, $M_x N_x - M_y N_y$	✗
D_{4h}	A_{2g}	$k_x k_y (k_x^2 - k_y^2)$	$M_x N_y - M_y N_x$	✓
D_{4h}	B_{1g}	$k_x^2 - k_y^2$	$M_x N_x - M_y N_y$	✗
D_{4h}	B_{2g}	$k_x k_y$	$M_x N_y + M_y N_x$	✗
D_{3d}	A_{2g}	$k_x k_z (k_x^2 - 3k_y^2)$	$M_x N_y - M_y N_x$	✓
C_{6h}	B_g	$\alpha k_y k_z (k_y^2 - 3k_x^2)$ $+\beta k_x k_z (k_x^2 - 3k_y^2)$	$\alpha M_z N_y (3N_x^2 - N_y^2)$ $+\beta M_z N_x (3N_y^2 - N_x^2)$	✗
D_{6h}	A_{2g}	$k_x k_y (k_x^2 - 3k_y^2)$ $\times (k_y^2 - 3k_x^2)$	$M_x N_y - M_y N_x$	✓
D_{6h}	B_{1g}	$k_y k_z (3k_x^2 - k_y^2)$	$M_z N_y (3N_x^2 - N_y^2)$	✗
D_{6h}	B_{2g}	$k_x k_z (k_x^2 - 3k_y^2)$	$M_z N_x (N_x^2 - 3N_y^2)$	✗
O_h	A_{2g}	$k_x^4 (k_y^2 - k_z^2)$ $+k_y^4 (k_z^2 - k_x^2)$ $+k_z^4 (k_x^2 - k_y^2)$	$M_x N_x (N_y^2 - N_z^2)$ $+M_y N_y (N_z^2 - N_x^2)$ $+M_z N_z (N_x^2 - N_y^2)$	✗

Initially, we analyze the AHE. For the Néel order along an arbitrary direction l, N_l, the only contribution to the Berry curvature that is linear in SOC originates from the SOC component parallel to l, that is λ_l, and is given by [35,39]

$$\Omega^{(N_l)}_{\alpha,\beta,ij} = \frac{1}{2E^3_{\alpha,\beta}} \sum_{m,n=i,j} \varepsilon_{mn} \Big[(N_l + \beta|t_{z,\mathbf{k}}|)\partial_m \lambda_{l,\mathbf{k}} \partial_n t_{x,\mathbf{k}} + \mathrm{sgn}(t_{z,\mathbf{k}})\beta t_{x,\mathbf{k}} \partial_m t_{z,\mathbf{k}} \partial_n \lambda_{l,\mathbf{k}} + \mathrm{sgn}(t_{z,\mathbf{k}})\beta \lambda_{l,\mathbf{k}} \partial_m t_{x,\mathbf{k}} \partial_n t_{z,\mathbf{k}} \Big], \quad (3)$$

where the dispersion is $E_{\alpha=\pm,\beta=\pm} = \alpha\Big(N_l^2 + \lambda_{l,\mathbf{k}}^2 + t_{x,\mathbf{k}}^2 + t_{z,\mathbf{k}}^2 + 2\beta|N_l||t_{z,\mathbf{k}}|\Big)^{1/2}$. This expression is generically nonzero. Thus, when allowed by symmetry, the AHE is

expected to be large and linear in SOC for all point groups and AM symmetries. In SM [39], we carry out calculations of the AHE that support this conclusion.

To study now the interplay of the Néel order $\vec{N}$ and the induced $\vec{M}$, we consider the perturbation

$$H' = \tau_z \vec{N} \cdot \vec{\sigma} + \vec{M} \cdot \vec{\sigma} \tag{4}$$

to the normal state Hamiltonian. We calculate the corrections to the normal state free energy close to the critical temperature as the magnetic order sets in by evaluating the loop expansion of the free energy. To the second order it reads as

$$F^{(2)} = \frac{1}{2\beta} \sum_{i\omega_n} \mathrm{Tr}[G_0 H' G_0 H']. \tag{5}$$

Here, the bare Green's function projected to the band basis is given by

$$G_0(\mathbf{k}, i\omega_n) = \sum_{a=\pm} G_0^a(\mathbf{k}, i\omega_n) |u_{\mathbf{k}}^a\rangle\langle u_{\mathbf{k}}^a|, \tag{6}$$

where $G_0^{(\pm)}(\mathbf{k}, i\omega_n) = \{1/[i\omega_n - (\varepsilon_{0,\mathbf{k}} \pm \tilde{E}_{\mathbf{k}})]\}$ denotes the Green's function in the band basis, with the twofold degenerate eigenenergies $E_{\mathbf{k}}^{\pm} = \varepsilon_{0,\mathbf{k}} \pm \tilde{E}_{\mathbf{k}}$ with $\tilde{E}_{\mathbf{k}} = \sqrt{t_{x,\mathbf{k}}^2 + t_{z,\mathbf{k}}^2 + \vec{\lambda}_{\mathbf{k}}^2}$. The projection operator $P_{\mathbf{k}}^a = |u_{\mathbf{k}}^a\rangle\langle u_{\mathbf{k}}^a|$ in Eq. (6) transforms from the sublattice basis onto band a at wave vector $\mathbf{k}$ [39,43].

To examine the bilinear coupling between $\vec{N}$ and $\vec{M}$, we derive an expression for the coefficient c_{ij} in Eq. (1). The analytic expressions for the other coefficients in Eq. (1) can be found in SM [39]. At the one-loop level, the quadratic free energy contribution in Eq. (5) coupling $\vec{M}$ and $\vec{N}$ is given by

$$F_{NM}^{(2)} = \frac{1}{\beta} \mathrm{Tr} \left[\sum_{a,b,i\omega_n} G^a(\mathbf{k}, i\omega_n) G^b(\mathbf{k}, i\omega_n) \tau_z \vec{N} \cdot \vec{\sigma} P_{\mathbf{k}}^a \vec{M} \cdot \vec{\sigma} P_{\mathbf{k}}^b \right]. \tag{7}$$

Calculating the trace and performing the Matsubara frequency sum, we obtain

$$F_{NM}^{(2)} = 2 \sum_{\mathbf{k}} \frac{t_{x,\mathbf{k}}}{\tilde{E}_{\mathbf{k}}^2} L(\mathbf{k}) \vec{\lambda}_{\mathbf{k}} \cdot (\vec{M} \times \vec{N}), \tag{8}$$

with the function

$$L(\mathbf{k}) = \left. \frac{df(\varepsilon)}{d\varepsilon} \right|_{\varepsilon = E_{\mathbf{k}}^+} + \left. \frac{df(\varepsilon)}{d\varepsilon} \right|_{\varepsilon = E_{\mathbf{k}}^-} - \frac{2[f(E_{\mathbf{k}}^-) - f(E_{\mathbf{k}}^+)]}{E_{\mathbf{k}}^- - E_{\mathbf{k}}^+}, \tag{9}$$

incorporating the density of states and Lindhard term. The combination $(\vec{M} \times \vec{N})$ in Eq. (8) reveals that a nonzero invariant exists only if the antisymmetric direct product of the two axial IRs $[\Gamma_A \otimes \Gamma_A]_-$ contains Γ_N. In Table I we list whether the invariant can be generated to linear order of SOC; the antisymmetric product for the different point groups is detailed in SM [39]. The SOC is expected to be a weak effect in AM [19], and therefore the induced magnetization will be vanishingly small when it is not generated to linear order. As seen from Table I, for the point group D_{4h} the SOC-linear invariant is only generated for $\Gamma_N = A_{2g}$. Focusing on crystals with a rutile structure, i.e., space group (SG) 136 and Wyckoff position 2a for the magnetic atoms as in RuO_2, MnF_2, NiF_2, and CoF_2, we have $\Gamma_N = B_{2g}$. Consequently, the induced $\vec{M}$ is at least quadratic in SOC, as opposed to the material candidates Nb_2FeB_2 and Ta_2FeB_2, which have $\Gamma_N = A_{2g}$. Notably, Table I also shows that the FM moment induced in orthorhombic materials (D_{2h}) is generally expected to be larger.

To further verify these points, in Fig. 1 we show the calculated $\vec{M} = \mu_B \sum_{a,\mathbf{k}} \langle u_{\mathbf{k}}^a | \vec{S} | u_{\mathbf{k}}^a \rangle f(E_{\mathbf{k}}^a)$ relevant for (a) rutile structure (D_{4h}, $\Gamma_N = B_{2g}$) and (b) $FeSb_2$ structure (D_{2h}, $\Gamma_N = B_{1g}$). As seen, the SOC-induced $\vec{M}$ indeed scales quadratically (linearly) with the SOC strength for SG 136 ($FeSb_2$) and is significantly smaller for the band relevant for rutile AM compared to $FeSb_2$. For the case of $FeSb_2$ we additionally compare the induced $\vec{M}$ for the Néel vector along the x axis and the y axis in Fig. 1(d) to see if $\vec{M}$ follows the predicted microscopic $(M_x N_y - M_y N_x)$ result for the invariant. Indeed, even though M_x and M_y are not symmetry related in this orthorhombic system, they are of opposite sign and nearly identical in magnitude for this material. In summary, these results explicitly demonstrate the properties summarized in Table I, which can be applied to gain similar insight for many classes of AM materials.

Finally, we note that, in order to understand the quadratic dependence of $\vec{M}$ on SOC from exact diagonalization, when $\vec{M}$ is not allowed to linear order, requires the inclusion of secondary order parameters [23], equivalent to two-loop calculations [39]. Specifically, when AM order sets in, secondary order parameters are also induced by symmetry, and they can give rise to a finite coupling between the two orders $\vec{M}$ and $\vec{N}$. Such secondary order parameters include other spin textures as well as a current loop order; see SM [39]. The free energy for a secondary order parameter $\vec{O}$ can be written as

$$F = \gamma^{(1)} \vec{O}^2 + \gamma_{ij}^{(2)} N_i O_j + \gamma_{ij}^{(3)} M_i O_j, \tag{10}$$

which couples bilinearly to $\vec{M}$ and $\vec{N}$. Thus, $\vec{N}$ can also induce a magnetization $\vec{M}$ through the secondary order parameter $\vec{O}$, and our minimal models reveal that in this case the FM spin moment is at least quadratic in SOC, as discussed in SM [39].

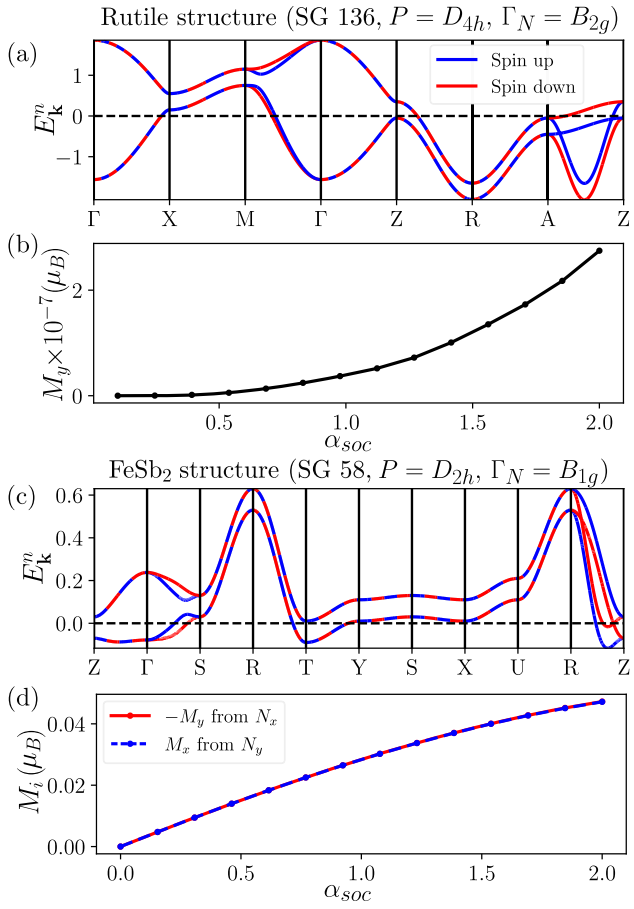

FIG. 1. Minimal model band structures and induced magnetization as a function of SOC strength for RuO_2 (a),(b) vs $FeSb_2$ (c),(d). We take $\vec{\lambda} = \alpha_{\rm soc}\vec{\lambda}_0$, with $\vec{\lambda}_0 = (0.05, 0.05, 0.17)$ eV and $N_x = 0.2$ for RuO_2, and $\vec{\lambda}_0 = (2.7, 6.6, 75)$ meV and $N_x = 0.05$ for $FeSb_2$, both estimated from DFT results (see SM [39]). In agreement with Table I, $\vec{M}$ is induced along the y axis for N_x, and scales quadratically (linearly) with the SOC strength for RuO_2 ($FeSb_2$). In (d) we show also the case with the Néel vector along the y axis N_y, inducing $M_x \simeq -M_y$.

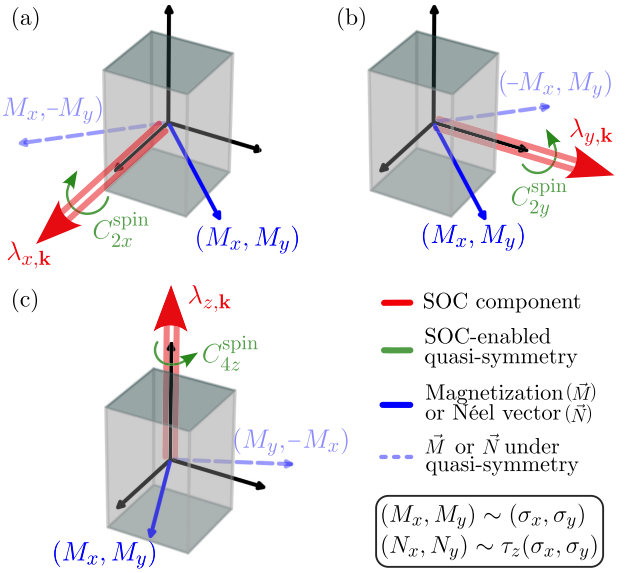

FIG. 2. SOC-enabled quasisymmetry in a tetragonal system when only a single SOC component (a) $\lambda_{x,\mathbf{k}}$, (b) $\lambda_{y,\mathbf{k}}$, or (c) $\lambda_{z,\mathbf{k}}$ is present. The quasisymmetry acts only in spin space, transforming the magnetization $\vec{M}$ and the spin components of the Néel vector $\vec{N}$ in the same way.

Quasisymmetry protection of negligible FM—Our minimal models are in agreement with the DFT results, which suggests a more general explanation beyond specific loop expansions or microscopic models. Indeed, it is possible to understand the above results using the recently introduced concept of quasisymmetry [36,37], describing emergent approximate symmetries when certain terms in the Hamiltonian become negligible. Here we use SOC to generate our quasisymmetry. Specifically, we consider the quasisymmetry that emerges when two of the SOC components (λ_x, λ_y, or λ_z) vanish, as illustrated in Fig. 2 for a tetragonal system. The resulting symmetry group, which we denote the uniaxial spin space group due to its spin rotational invariance around the SOC direction, has higher symmetry than the magnetic space group but lower symmetry than the spin space group. This is relevant for determining which Landau coefficients are linear in one of $\lambda_{x,y,z}$. For example, for $\lambda_z \neq 0$ with $\lambda_x = \lambda_y = 0$, the normal state Hamiltonian gains additional symmetries, i.e., quasisymmetries. Importantly, whether the λ_z-linear contribution to the Landau coefficient is permitted depends not only on the intrinsic symmetries of the crystal but also on these emergent quasisymmetries [36,37].

Here, we apply this to the Landau coefficients of M_xN_y and M_yN_x. When only λ_x (λ_y) SOC is present, the normal state Hamiltonian acquires an additional twofold spin-rotational symmetry $[C_{2x}\|E]$ ($[C_{2y}\|E]$), see Fig. 2(a) [Fig. 2(b)], which prohibits the λ_x- [or λ_y-] linear contribution to these two Landau coefficients since M_x [N_x] is odd under this quasisymmetry while N_y [M_y] is even. When only λ_z is present, a relevant quasisymmetry in the uniaxial spin point group is the fourfold spin-rotational symmetry $[C_{4z}\|E]$. As seen from Fig. 2(c), under this symmetry the SOC-linear contribution to M_xN_y and M_yN_x coefficients must have opposite signs. This behavior is universal and applies to any space group, regardless of whether it has intrinsic fourfold rotational symmetry, as demonstrated in Fig. 1(d) for $FeSb_2$. In structures with SG 136, however, its intrinsic tetragonal crystal symmetries force these two coefficients to be identical at all orders of SOC. Consequently, the SOC-linear contribution must vanish, as shown in Fig. 1(b). The complete discussion on other space groups can be found in SM [39]. This also implies that for MnTe and CrSb, which have point group D_{6h} and $\Gamma_N = B_{1g}$, the FM moment will be cubic in SOC (see End Matter), independent of the nonlinear coupling

terms in Table I, in agreement with Refs. [27,31]. Hence, the SOC enabled quasisymmetry demonstrates that the results of the microscopic model are very general and naturally explains when the FM spin moment is large or small depending on the AM symmetry. The only assumption on the microscopic Hamiltonian that underlies this analysis is that AM is an instability purely in the spin channel, that is, it is driven only by exchange interactions without any orbital angular momentum contribution.

The relationship between the SOC direction and nonvanishing AHE in Eq. (3) can also be understood using SOC-based quasisymmetry arguments like those given above, which do not depend on the form of the microscopic model. Specifically, the AHE measures current and voltage response and hence is even under spin-rotational symmetries. For the Néel order along $\hat{x}$, when only the λ_y (λ_z) SOC is kept, the Néel order is odd under the resulting quasi-spin-rotational symmetry $[C_{2y}\|E]$ ($[C_{2z}\|E]$). This prevents a λ_y (λ_z)-linear SOC contribution to the AHE. When only the λ_x SOC is kept, the Néel order is even under the resulting $[C_{2x}\|E]$ symmetry, and therefore the λ_x-linear contribution to AHE is allowed by the quasisymmetry. It naturally follows that the AHE is given by the SOC component that is parallel to the Néel vector.

Magnetic anisotropy energy—The presence of SOC leads to a preferred direction for the Néel vector. As seen from the free energy in Eq. (1), this is captured by the s_1 and s_2 Landau coefficients. Thus, deriving analytic expressions for these coefficients from the microscopic models is useful to providing insight into the easy axis direction. Using the general microscopic model in Eq. (2) and focusing on the quadratic free energy correction due to SOC [see Eq. (5)], the coefficients can be written as

$$s_1 = -\frac{1}{2}\sum_{\mathbf{k}} \frac{\lambda_{x,\mathbf{k}}^2 - \lambda_{y,\mathbf{k}}^2}{\tilde{E}_{\mathbf{k}}^2} L(\mathbf{k}), \tag{11}$$

$$s_2 = -\frac{1}{6}\sum_{\mathbf{k}} \frac{\lambda_{x,\mathbf{k}}^2 + \lambda_{y,\mathbf{k}}^2 - 2\lambda_{z,\mathbf{k}}^2}{\tilde{E}_{\mathbf{k}}^2} L(\mathbf{k}), \tag{12}$$

with the function $L(\mathbf{k})$ defined in Eq. (9). The sign of these coefficients fixes the easy axis for a specific AM material. For instance, focusing on SG 136, $\lambda_{z,\mathbf{k}}$ can be ignored as it is smaller than $\lambda_{x,\mathbf{k}}$ and $\lambda_{y,\mathbf{k}}$ [35]. Hence, in general we expect that $s_2 > 0$, and as a consequence, the easy axis is out of plane. However, Eqs. (11) and (12) also reveal that the moment direction may switch depending on the Fermi energy. In particular, when the Lindhard function [interband term in $L(\mathbf{k})$] dominates over the density of states (intraband term), $L(\mathbf{k})$ can change sign leading to $s_2 < 0$ and in-plane moment orientation. The switch of the AM moments as a function of the Fermi energy from the c axis to the in-plane direction has been reported in Ref. [15] for RuO_2. As shown in SM, calculations of s_1 and s_2 for a minimal model of RuO_2 indeed yield $s_1 = 0$, $s_2 > 0$. In addition, application to $FeSb_2$ reveal that $s_1 > 0$, $s_2 < 0$, i.e., moments aligned along the in-plane y axis, in agreement with DFT studies [32]. A systematic application of the magnetic anisotropy energy based on Eqs. (11) and (12) to other AM is beyond the scope of this Letter and constitutes an interesting future project.

Conclusions—In summary, we have applied recently developed realistic microscopic models for AM to derive relevant Landau coefficients of the free energy, focusing on the coupling between magnetization and Néel order, and magnetic anisotropy energies. The results explain the generic large AHE and the observed strong material dependence of the SOC-induced weak FM. We stress that the weak FM described in this Letter refers to the spin moment. For materials where this moment is forbidden to linear order, e.g., the rutiles, secondary orders become relevant, and the orbital magnetic moment may also yield contributions to the small but finite net magnetization [18,44]. Finally, we discovered a general quasisymmetry enabled by the SOC that is model independent and allows for determining for which AM symmetries the induced FM spin moment is large or vanishingly small.

Acknowledgments—M. R. acknowledges support from the Novo Nordisk Foundation under Grant No. NNF20OC0060019. A. K. acknowledges support by the Danish National Committee for Research Infrastructure (NUFI) through the ESS-Lighthouse Q-MAT. D. F. A. and Y. Y. were supported by the National Science Foundation under Grant No. DMREF 2323857. Work at UWM was also supported by the Simons Foundation under Grant No. SFI-MPS-NFS-00006741-02 (D. F. A and M. R.).

Data availability—The data are not publicly available. The data are available from the authors upon reasonable request.

[1] Naoto Nagaosa, Jairo Sinova, Shigeki Onoda, A. H. MacDonald, and N. P. Ong, Anomalous Hall effect, Rev. Mod. Phys. **82**, 1539 (2010).

[2] Inti Sodemann and Liang Fu, Quantum nonlinear Hall effect induced by Berry curvature dipole in time-reversal invariant materials, Phys. Rev. Lett. **115**, 216806 (2015).

[3] Anyuan Gao, Yu-Fei Liu, Jian-Xiang Qiu, Barun Ghosh, Thaís V. Trevisan, Yugo Onishi, Chaowei Hu, Tiema Qian, Hung-Ju Tien, Shao-Wen Chen, Mengqi Huang, Damien Bérubé, Houchen Li, Christian Tzschaschel, Thao Dinh *et al.*, Quantum metric nonlinear Hall effect in a topological antiferromagnetic heterostructure, Science **381**, 181 (2023).

[4] Daniel Kaplan, Tobias Holder, and Binghai Yan, Unification of nonlinear anomalous Hall effect and nonreciprocal magnetoresistance in metals by the quantum geometry, Phys. Rev. Lett. **132**, 026301 (2024).

[5] Yuan Fang, Jennifer Cano, and Sayed Ali Akbar Ghorashi, Quantum geometry induced nonlinear transport in altermagnets, Phys. Rev. Lett. **133**, 106701 (2024).
[6] Z. Z. Du, Hai-Zhou Lu, and X. C. Xie, Nonlinear Hall effects, Nat. Rev. Phys. **3**, 744 (2021).
[7] Naizhou Wang, Daniel Kaplan, Zhaowei Zhang, Tobias Holder, Ning Cao, Aifeng Wang, Xiaoyuan Zhou, Feifei Zhou, Zhengzhi Jiang, Chusheng Zhang, Shihao Ru, Hongbing Cai, Kenji Watanabe, Takashi Taniguchi, Binghai Yan, and Weibo Gao, Quantum-metric-induced nonlinear transport in a topological antiferromagnet, Nature (London) **621**, 487 (2023).
[8] Suyoung Lee, Sangjae Lee, Saegyeol Jung, Jiwon Jung, Donghan Kim, Yeonjae Lee, Byeongjun Seok, Jaeyoung Kim, Byeong Gyu Park, Libor Šmejkal, Chang-Jong Kang, and Changyoung Kim, Broken Kramers degeneracy in altermagnetic MnTe, Phys. Rev. Lett. **132**, 036702 (2024).
[9] J. Krempaský *et al.*, Altermagnetic lifting of Kramers spin degeneracy, Nature (London) **626**, 517 (2024).
[10] T. Osumi, S. Souma, T. Aoyama, K. Yamauchi, A. Honma, K. Nakayama, T. Takahashi, K. Ohgushi, and T. Sato, Observation of a giant band splitting in altermagnetic MnTe, Phys. Rev. B **109**, 115102 (2024).
[11] Cong Li, Mengli Hu, Zhilin Li, Yang Wang, Wanyu Chen, Balasubramanian Thiagarajan, Mats Leandersson, Craig Polley, Timur Kim, Hui Liu, Cosma Fulga, Maia G. Vergniory, Oleg Janson, Oscar Tjernberg, and Jeroen van den Brink, Topological Weyl altermagnetism in CrSb, arXiv:2405.14777.
[12] Guowei Yang *et al.*, Three-dimensional mapping of the altermagnetic spin splitting in CrSb, Nat. Commun. **16**, 1442 (2025).
[13] Sonka Reimers, Lukas Odenbreit, Libor Šmejkal, Vladimir N. Strocov, Procopios Constantinou, Anna B. Hellenes, Rodrigo Jaeschke Ubiergo, Warlley H. Campos, Venkata K. Bharadwaj, Atasi Chakraborty, Thibaud Denneulin, Wen Shi, Rafal E. Dunin-Borkowski, Suvadip Das, Mathias Kläui, Jairo Sinova, and Martin Jourdan, Direct observation of altermagnetic band splitting in CrSb thin films, Nat. Commun. **15**, 1 (2024).
[14] Jianyang Ding *et al.*, Large band splitting in g-wave altermagnet CrSb, Phys. Rev. Lett. **133**, 206401 (2024).
[15] Zexin Feng, Xiaorong Zhou, Libor Šmejkal, Lei Wu, Zengwei Zhu, Huixin Guo, Rafael González-Hernández, Xiaoning Wang, Han Yan, Peixin Qin, Xin Zhang, Haojiang Wu, Hongyu Chen, Ziang Meng, Li Liu, Zhengcai Xia, Jairo Sinova, Tomáš Jungwirth, and Zhiqi Liu, An anomalous Hall effect in altermagnetic ruthenium dioxide, Nat. Electron. Rev. **5**, 735 (2022).
[16] K. P. Kluczyk, K. Gas, M. J. Grzybowski, P. Skupiński, M. A. Borysiewicz, T. Fas, J. Suffczyński, J. Z. Domagala, K. Grasza, A. Mycielski, M. Baj, K. H. Ahn, K. Výborný, M. Sawicki, and M. Gryglas-Borysiewicz, Coexistence of anomalous Hall effect and weak magnetization in a nominally collinear antiferromagnet MnTe, Phys. Rev. B **110**, 155201 (2024).
[17] R. D. Gonzalez Betancourt, J. Zubáč, R. Gonzalez-Hernandez, K. Geishendorf, Z. Šobáň, G. Springholz, K. Olejník, L. Šmejkal, J. Sinova, T. Jungwirth, S. T. B. Goennenwein, A. Thomas, H. Reichlová, J. Železný, and D. Kriegner, Spontaneous anomalous Hall effect arising from an unconventional compensated magnetic phase in a semiconductor, Phys. Rev. Lett. **130**, 036702 (2023).
[18] Libor Šmejkal, Rafael González-Hernández, T. Jungwirth, and J. Sinova, Crystal time-reversal symmetry breaking and spontaneous Hall effect in collinear antiferromagnets, Sci. Adv. **6**, eaaz8809 (2020).
[19] Libor Šmejkal, Jairo Sinova, and Tomas Jungwirth, Beyond conventional ferromagnetism and antiferromagnetism: A phase with nonrelativistic spin and crystal rotation symmetry, Phys. Rev. X **12**, 031042 (2022).
[20] Libor Šmejkal, Jairo Sinova, and Tomas Jungwirth, Emerging research landscape of altermagnetism, Phys. Rev. X **12**, 040501 (2022).
[21] Libor Šmejkal, Allan H. MacDonald, Jairo Sinova, Satoru Nakatsuji, and Tomas Jungwirth, Anomalous Hall antiferromagnets, Nat. Rev. Mater. **7**, 482 (2022).
[22] Hai-Yang Ma, Mengli Hu, Nana Li, Jianpeng Liu, Wang Yao, Jin-Feng Jia, and Junwei Liu, Multifunctional antiferromagnetic materials with giant piezomagnetism and noncollinear spin current, Nat. Commun. **12**, 1 (2021).
[23] Paul A. McClarty and Jeffrey G. Rau, Landau theory of altermagnetism, Phys. Rev. Lett. **132**, 176702 (2024).
[24] Rui-Chun Xiao, Hui Li, Hui Han, Wei Gan, Mengmeng Yang, Ding-Fu Shao, Shu-Hui Zhang, Yang Gao, Mingliang Tian, and Jianhui Zhou, Anomalous-Hall Neel textures in altermagnetic materials, arXiv:2411.10147.
[25] Rafael M. Fernandes, Vanuildo S. de Carvalho, Turan Birol, and Rodrigo G. Pereira, Topological transition from nodal to nodeless Zeeman splitting in altermagnets, Phys. Rev. B **109**, 024404 (2024).
[26] Sang-Wook Cheong and Fei-Ting Huang, Altermagnetism with non-collinear spins, npj Quantum Mater. **9**, 1 (2024).
[27] I. I. Mazin and K. D. Belashchenko, Origin of the gossamer ferromagnetism in MnTe, Phys. Rev. B **110**, 214436 (2024).
[28] T. Berlijn, P. C. Snijders, O. Delaire, H.-D. Zhou, T. A. Maier, H.-B. Cao, S.-X. Chi, M. Matsuda, Y. Wang, M. R. Koehler, P. R. C. Kent, and H. H. Weitering, Itinerant antiferromagnetism in RuO_2, Phys. Rev. Lett. **118**, 077201 (2017).
[29] M. Hiraishi, H. Okabe, A. Koda, R. Kadono, T. Muroi, D. Hirai, and Z. Hiroi, Nonmagnetic ground state in RuO_2 revealed by muon spin rotation, Phys. Rev. Lett. **132**, 166702 (2024).
[30] Philipp Keßler, Laura Garcia-Gassull, Andreas Suter, Thomas Prokscha, Zaher Salman, Dmitry Khalyavin, Pascal Manuel, Fabio Orlandi, Igor I. Mazin, Roser Valentí, and Simon Moser, Absence of magnetic order in RuO_2: Insights from μSR spectroscopy and neutron diffraction, npj Spintronics **2**, 50 (2024).
[31] Carmine Autieri, Raghottam M. Sattigeri, Giuseppe Cuono, and Amar Fakhredine, Staggered Dzyaloshinskii-Moriya interaction inducing weak ferromagnetism in centrosymmetric altermagnets and weak ferrimagnetism in noncentrosymmetric altermagnets, Phys. Rev. B **111**, 054442 (2025).
[32] Igor I. Mazin, Klaus Koepernik, Michelle D. Johannes, Rafael González-Hernández, and Libor Šmejkal, Prediction of unconventional magnetism in doped $FeSb_2$, Proc. Natl. Acad. Sci. U.S.A. **118**, e2108924118 (2021).

[33] Lotan Attias, Alex Levchenko, and Maxim Khodas, Intrinsic anomalous Hall effect in altermagnets, Phys. Rev. B **110**, 094425 (2024).
[34] Marko Milivojević, Marko Orozović, Silvia Picozzi, Martin Gmitra, and Srđan Stavrić, Interplay of altermagnetism and weak ferromagnetism in two-dimensional RuF_4, 2D Mater. **11**, 035025 (2024).
[35] Mercè Roig, Andreas Kreisel, Yue Yu, Brian M. Andersen, and Daniel F. Agterberg, Minimal models for altermagnetism, Phys. Rev. B **110**, 144412 (2024).
[36] Jiayu Li, Ao Zhang, Yuntian Liu, and Qihang Liu, Group theory on quasisymmetry and protected near degeneracy, Phys. Rev. Lett. **133**, 026402 (2024).
[37] Chunyu Guo, Lunhui Hu, Carsten Putzke, Jonas Diaz, Xiangwei Huang, Kaustuv Manna, Feng-Ren Fan, Chandra Shekhar, Yan Sun, Claudia Felser, Chaoxing Liu, B. Andrei Bernevig, and Philip J. W. Moll, Quasi-symmetry-protected topology in a semi-metal, Nat. Phys. **18**, 813 (2022).
[38] Xiao-Yao Hou, Huan-Cheng Yang, Zheng-Xin Liu, Peng-Jie Guo, and Zhong-Yi Lu, Large intrinsic anomalous Hall effect in both Nb_2FeB_2 and Ta_2FeB_2 with collinear antiferromagnetism, Phys. Rev. B **107**, L161109 (2023).
[39] See Supplemental Material at http://link.aps.org/supplemental/10.1103/839n-rckn for quasisymmetry constrained spin ferromagnetism in altermagnets.
[40] Matthias Hecker, Anant Rastogi, Daniel F. Agterberg, and Rafael M. Fernandes, Classification of electronic nematicity in three-dimensional crystals and quasicrystals, Phys. Rev. B **109**, 235148 (2024).
[41] Satoru Hayami, Megumi Yatsushiro, Yuki Yanagi, and Kusunose Hiroaki, Classification of atomic-scale multipoles under crystallographic point groups and application to linear response tensors, Phys. Rev. B **98**, 165110 (2018).
[42] Sayantika Bhowal and Nicola A. Spaldin, Ferroically ordered magnetic octupoles in d-wave altermagnets, Phys. Rev. X **14**, 011019 (2024).
[43] Ansgar Graf and Frédéric Piéchon, Berry curvature and quantum metric in N-band systems: An eigenprojector approach, Phys. Rev. B **104**, 085114 (2021).
[44] Daegeun Jo, Dongwook Go, Yuriy Mokrousov, Peter M. Oppeneer, Sang-Wook Cheong, and Hyun-Woo Lee, Weak ferromagnetism in altermagnets from alternating g-tensor anisotropy, Phys. Rev. Lett. **134**, 196703 (2025).

End Matter

Appendix A: General SOC-enabled quasisymmetry—As introduced in the main text, the quasisymmetry generated by SOC when two of the SOC components vanish allows us to determine which Landau coefficients are linear in one of $\lambda_{x,y,z}$. As illustrated in Fig. 3, the resulting symmetry group, denoted here as the uniaxial spin space group, has lower symmetry than the spin space group but higher symmetry than the magnetic space group. Here, we develop a more general quasisymmetry criterion that addresses the following question: can a Landau coefficient or response function host a contribution from $\lambda_x^{n_x}\lambda_y^{n_y}\lambda_z^{n_z}$, for given integers $(n_x, n_y, n_z) \geq 0$?

We would like to consider a general Hamiltonian that can extend beyond the minimal models discussed in this Letter. SOC terms can always be grouped into terms proportional to spin operators σ_x, σ_y, and σ_z. Terms in each group can carry different momentum and orbital dependence, with overall SOC strengths λ_x, λ_y, and λ_z:

$$\begin{aligned} H_{SOC} = {} & \lambda_x(a_{1,\mathbf{k}}\widehat{A_1} + a_{2,\mathbf{k}}\widehat{A_2} + \cdots)\sigma_x \\ & + \lambda_y(b_{1,\mathbf{k}}\widehat{B_1} + b_{2,\mathbf{k}}\widehat{B_2} + \cdots)\sigma_y \\ & + \lambda_z(c_{1,\mathbf{k}}\widehat{C_1} + c_{2,\mathbf{k}}\widehat{C_2} + \cdots)\sigma_z, \end{aligned} \tag{A1}$$

with momentum-dependent coefficients of $a_i, b_i, c_i = O(1)$ and $\widehat{A_i}$, $\widehat{B_i}$, $\widehat{C_i}$ being some operators acting on sublattice and/or orbital space. The quasisymmetry argument is based on the analyticity of the response functions. If the DOS is not concentrated at singular regions such as band crossings, response functions should be an analytical function of $\lambda_{x,y,z}$. Cross terms like $\sqrt{\lambda_x\lambda_y}$ are not allowed. For the minimal model, this property is explicitly shown in the normal state Green's function [Eq. (6)], where the projection operator is a linear combination of the three SOC terms.

We now interpret the three groups of SOC terms as distinct symmetry breaking order parameters in a SOC-free system (spin space group). The spin space group hosts

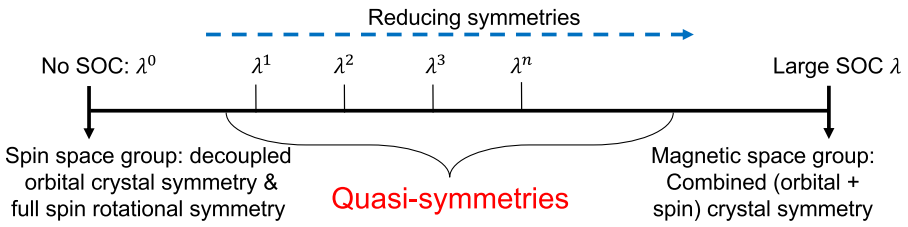

FIG. 3. Classification scheme of the spin space group and magnetic space group in terms of the strength and powers of SOC, illustrating when the quasisymmetries emerge. In particular, when two of the SOC components vanish, the resulting symmetry group (which we denote as the uniaxial spin space group) has spin rotational invariance around the SOC direction.

decoupled orbital crystal symmetries and full spin-rotational symmetries. General order parameters are denoted by $\vec{O}_{R,i}$, where R is the IR under orbital rotations and the index $i = 1, 2, \ldots$ reflects its dimensionality. The vector notation indicates that each $\vec{O}_{R,i}$ also transforms as a spin vector under spin rotations.

Each group of SOC terms corresponds to a different symmetry breaking in this high-symmetry system. For example, consider the λ_z SOC term in an tetragonal system. It breaks spin-rotational symmetry as the spin vector σ_z, and it breaks orbital symmetry according to the 1D IR $A_{2g} \sim xy(x^2 - y^2)$. It is then $\vec{O}_{A_{2g}} = (0, 0, \Lambda_z)$. For $\lambda_{x,y}$ SOC terms, they break spin-rotational symmetry as the spin vector $\sigma_{x,y}$, and they break orbital symmetry according to the 2D IR $E_g \sim \{xz, yz\}$. They are then $\vec{O}_{E_g,1} = (\Lambda_{xy}, 0, 0)$ and $\vec{O}_{E_g,2} = (0, \Lambda_{xy}, 0)$.

If the coefficient of a Landau term or response function X hosts a contribution from $\lambda_x^{n_x}\lambda_y^{n_y}\lambda_z^{n_z}$, then the term $\Lambda_x^{n_x}\Lambda_y^{n_y}\Lambda_z^{n_z}X$ must be allowed in the Landau theory for the SOC-free system. We note that for the tetragonal system, the contributions from $\lambda_{x,y}^{n_{xy}}\lambda_z^{n_z}$ enable the term $\Lambda_{xy}^{n_{xy}}\Lambda_z^{n_z}X$ in the Landau theory for the SOC-free system (since $\lambda_x = \lambda_y$ in this case). In the SOC-free system, a valid Landau term should be a spin scalar and belong to the trivial IR under orbital rotations. This provides a general quasisymmetry criterion.

Appendix B: Examples—In the SOC-free tetragonal D_{4h} systems, the SOC order parameters are $\vec{O}_{E_g,1} = (\Lambda_{xy}, 0, 0)$, $\vec{O}_{E_g,2} = (0, \Lambda_{xy}, 0)$, and $\vec{O}_{A_{2g}} = (0, 0, \Lambda_z)$. Ferromagnetic order is $\vec{M}_{A_{1g}}$, and altermagnetic order is $\vec{N}_P$, with altermagnetic symmetry $\Gamma_N = P$. To have a SOC-linear coupling between an altermagnet and a ferromagnet, $\vec{O} \cdot (\vec{M} \times \vec{N})$ must be allowed. The altermagnetic symmetry thus has to be A_{2g} or E_g. For two atoms per nonmagnetic unit cell, only $\Gamma_N = A_{2g}, B_{1g}, B_{2g}$ are allowed [35]. (1) For $\Gamma_N = A_{2g}$, the Landau term $\vec{O}_{A_{2g}} \cdot (\vec{M}_{A_{1g}} \times \vec{N}_{A_{2g}}) = \Lambda_z(M_xN_y - M_yN_x)$ is allowed. Hence the λ_z-linear contribution to $M_xN_y - M_yN_x$ is nonzero. (2) For $\Gamma_N = B_{2g}$ and Landau term $M_xN_y + M_yN_x$, SOC-linear terms are forbidden. Since $E_g \otimes E_g \otimes B_{2g}$ contains the trivial IR, the quadratic λ_{xy}^2 contribution is allowed. An example Landau term is $(\vec{O}_{E_g,1} \times \vec{M}) \cdot (\vec{N} \times \vec{O}_{E_g,2}) + (\vec{O}_{E_g,2} \times \vec{M}) \cdot (\vec{N} \times \vec{O}_{E_g,1}) = \Lambda_{xy}^2(M_xN_y + M_yN_x)$. (3) For $\Gamma_N = B_{1g}$ and Landau term $M_xN_x - M_yN_y$, SOC-linear terms are forbidden. Since $E_g \otimes E_g \otimes B_{1g}$ contains the trivial IR, the quadratic λ_{xy}^2 contribution is allowed. An example Landau term is $(\vec{O}_{E_g,1} \times \vec{M}) \cdot (\vec{N} \times \vec{O}_{E_g,1}) - (\vec{O}_{E_g,2} \times \vec{M}) \cdot (\vec{N} \times \vec{O}_{E_g,2}) = \Lambda_{xy}^2(M_xN_x - M_yN_y)$.

In the SOC-free hexagonal D_{6h} systems, the SOC order parameters are $\vec{O}_{E_{1g},1} = (\Lambda_{xy}, 0, 0)$, $\vec{O}_{E_{1g},2} = (0, \Lambda_{xy}, 0)$, and $\vec{O}_{A_{2g}} = (0, 0, \Lambda_z)$. To have a SOC-linear coupling between altermagnet and ferromagnet, $\vec{O} \cdot (\vec{M} \times \vec{N})$ must be allowed. Thus, $\Gamma_N = A_{2g}$ or E_{1g}. For two atoms per nonmagnetic unit cell, only A_{2g}, B_{1g}, and B_{2g} are allowed [35]. (1) The discussion for $\Gamma_N = A_{2g}$ is the same as A_{2g} in tetragonal systems. (2) For $\Gamma_N = B_{1g}$ (similar for $\Gamma_N = B_{2g}$), MN^3 coupling has no SOC-linear contribution since $B_{1g} \otimes B_{1g} \otimes B_{1g} \otimes \{E_{1g}, A_{2g}\}$ has no trivial IR. Similarly, SOC-quadratic contribution is also forbidden since $B_{1g} \otimes B_{1g} \otimes B_{1g} \otimes \{E_{1g}, A_{2g}\} \otimes \{E_{1g}, A_{2g}\}$ has no trivial IR. SOC-cubic contribution is allowed as $B_{1g} \otimes B_{1g} \otimes B_{1g} \otimes E_{1g} \otimes E_{1g} \otimes E_{1g}$ has trivial IR. The SOC dependence is cubic in λ_{xy}.

In the SOC-free cubic O_h systems, the SOC order parameters are $\vec{O}_{T_{1g},1} = (\Lambda, 0, 0)$, $\vec{O}_{T_{1g},2} = (0, \Lambda, 0)$, and $\vec{O}_{T_{1g},3} = (0, 0, \Lambda)$. For $\Gamma_N = A_{2g}$, MN^3 coupling has no SOC-linear contribution since $A_{2g} \otimes A_{2g} \otimes A_{2g} \otimes T_{1g}$ has no trivial IR. Similarly, a SOC-quadratic contribution is also forbidden since $A_{2g} \otimes A_{2g} \otimes A_{2g} \otimes T_{1g} \otimes T_{1g}$ has no trivial IR. Hence, the leading contribution is cubic in SOC, as $A_{2g} \otimes A_{2g} \otimes A_{2g} \otimes T_{1g} \otimes T_{1g} \otimes T_{1g}$ contains the trivial IR.